Robotica (2016) volume 34, pp. 913–924. © Cambridge University Press 2014
doi:10.1017/S0263574714001969

Stiffness and singularity analysis of foldable parallel mechanism for ship-based stabilized platform

Tie-shi Zhao†,‡,*, Chang Wang†,‡, Xiao Liu†,‡, Hui Bian†,‡ and Yan-zhi Zhao†,‡

†*Hebei Provincial Key Laboratory of Parallel Robot and Mechatronic System, Yanshan University, Qinhuangdao 066004, China*
‡*Key Laboratory of Advanced Forging & Stamping Technology and Science (Yanshan University), Ministry of Education of China, Qinhuangdao 066004, China*

(Accepted June 20, 2014. First published online: July 17, 2014)

SUMMARY
This paper investigates a 6-degree-of-freedom foldable parallel mechanism for the ship-based stabilized platform, which is driven by closed chain linkages. The velocity and acceleration mappings between the moving platform and inputs of the closed chain linkages are deduced in the form of the first- and second-order influence coefficient matrices. The continuous stiffness matrix is deduced; furthermore, the translation and rotational stiffness along any direction are also deduced. With directional stiffness, the singularity of the mechanism is analyzed, and the explanation of the singularity is given from the viewpoint of stiffness. The directions the platform cannot move or lose its constraints are got from directional stiffness.

KEYWORDS: Foldable parallel mechanism; Closed chain linkages; Stiffness; Singularity; Influence matrix.

1. Introduction

The role of a stabilized platform is to provide a relatively stable working environment for a bumpy carrier (like a ship, vehicle, *et al.*) to improve the operational accuracy and safety.[1–3] In recent years, much interest has been shown in stabilized platforms. However, most of these are 2-axis or 3-axis serial stabilized platforms whose bearing capacities are low, and they cannot counteract the motions of heave and sway. It has been noted that parallel mechanisms can realize multi-axis coupling motions and have the characteristics such as large bearing capacity and fast response,[4–6] so they are the ideal model for large-scale and multi-axis compensation stabilized platform. However, the application of the traditional Gough–Stewart platform is limited to structural height, so foldable parallel mechanism is considered. Most of the foldable mechanisms are better used in the situations that need to change the form[7,8] than those that need to output power. It is because foldable mechanism consists of lot of bars realizing foldable ability, which makes it easy to get into a singularity. The stoke output of foldable mechanism is generally larger than the input of drive, hence the stiffness of a foldable parallel is terrible without some reasonable processing.

The singularity is a very important parameter of mechanism. When a mechanism is in singularity, the degree-of-freedom (DOF) of mechanism changes instantaneously. Gosselin and Angeles[9] divided the singularity of closed-loop chains into three main groups. Zlatanov *et al.*[10,11] introduced a new classification and identification method for singular configurations of mechanisms. The classification of singularities is based on the physical phenomena that occur in singular configurations rather than that on the mathematical concept of degenerating Jacobians. Chung *et al*[12,13] proposed a new type of 3-DOF foldable parallel mechanism having three foldable sub-chains, and analyzed the singularity and drew singularity loci.

* Corresponding author. E-mail: tszhao@ysu.edu.cn

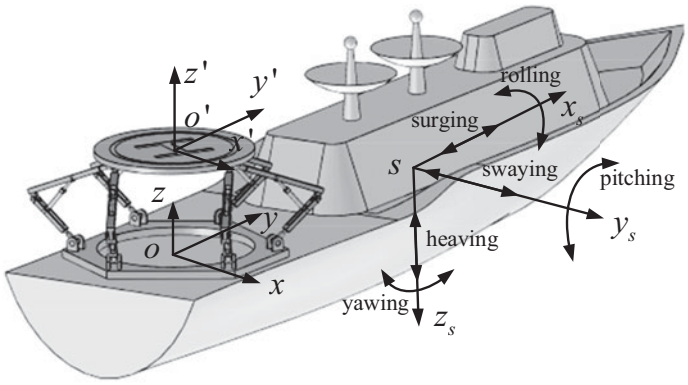

Fig. 1. Motions of a ship in the sea.

The stiffness expresses the bearing capacity. Joshi and Tsai[14] chose maximum and minimum stiffness as performance indexes, and concluded that tricept manipulator is better conditioned than 3-UPU manipulator. Shin *et al.*[15] introduced the stiffness analysis of the Eclipse-IA structure to examine the isotropy of stiffness matrix. Dai and Zhao[16] analyzed the stiffness characteristics of two-link under-actuated manipulators used in the virtual work principle, and illustrated the directional stiffness mapping.

The analysis of singularity and stiffness is based on mathematical derivation, which is precise and complex. However, this is not suitable for 6-DOF foldable parallel mechanism, whose kinematic clear expression is hard to obtain. Hence, the numerical method to judge the determinant of the Jacobian is taken to estimate singularity. Both singularity and stiffness are closely related to the Jacobian. Therefore, when the mechanism is in singularity, its stiffness must be special.

This paper mainly studies a 6-DOF mechanism of a ship-based stabilized platform, which can suffer heavy load. The relationship between the directional stiffness and the singularity of the mechanism is analyzed. In order to evaluate the bearing capacity around rotational and translational directions, the stiffness matrix is decomposed into rotational and translational stiffness considering the interaction of rotation and translation of a moving platform. After that the direction (including rotation and translation) that the mechanism cannot move or lose its constraints can be easily shown in the map of directional stiffness. The significance is that the singularity is illustrated in the form of directional stiffness.

2. Foldable Parallel Mechanism and its Kinematics

2.1. Description of mechanisms

As shown in Fig. 1, the movement of a ship is very complex as the wave in the sea is random. The ship's movements are rolling, pitching, yawing, surging, swaying, and heaving. Therefore, it needs a 6-DOF mechanism to isolate all these movements. In order to avoid the structural height restriction, the mechanisms are designed to be foldable. Figures 2(a) and (b) show the unfolded and folded states respectively. Meanwhile the closed chain drives are used to increase mechanism's stiffness, as the linear drives are easy to produce high stiffness by using screws. According to the closed chain, the rotation of middle joint is driven by the translation drive, as shown in Fig. 2.

The mechanism contains six branches that are distributed regularly around the vertical axis of a fixed platform. The axes (arrows on A_i ($i = 1,\ 2 \ldots 6$)) of the U-joint's first revolute joint is distributed, as illustrated in Fig. 3. The axes of the U-joint's second revolute joint points to the R-joint axes and vertical to it, as shown in Fig. 2(a).

2.2. Inverse kinematics

The sketch of a foldable parallel mechanism is illustrated in Fig. 3. Let A_i ($i = 1,\ 2 \ldots 6$) denote the central point of the U-joint connected to a fixed platform; subscript i stands for the ith branch; B_i is the center point of the joint between two bars; C_i is the center point of the sphere joint connected

https://doi.org/10.1017/S0263574714001969 Published online by Cambridge University Press

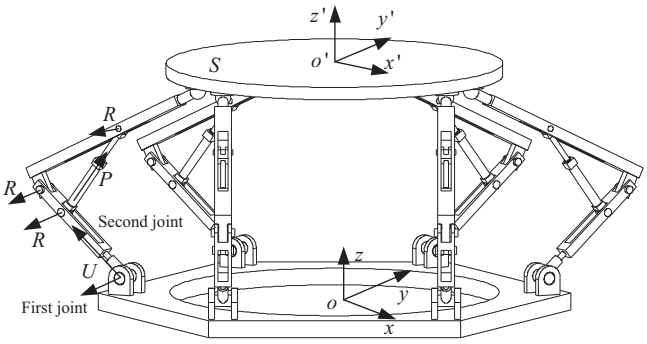

(a) Unfolded state

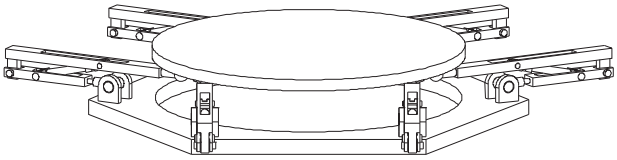

(b) Folded state

Fig. 2. Foldable parallel mechanism configurations.

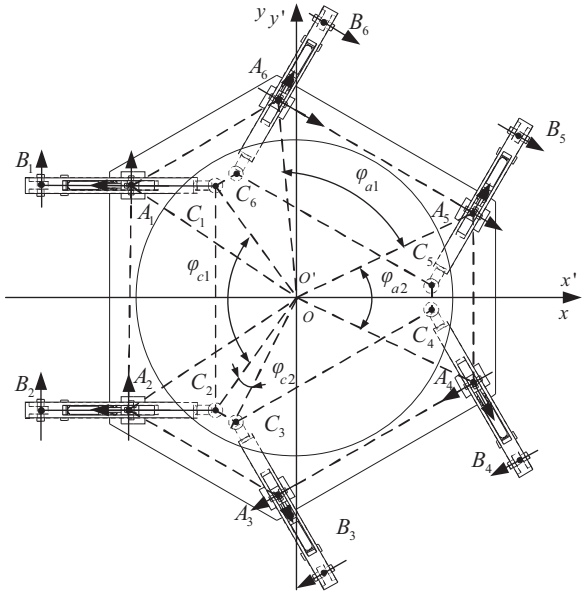

Fig. 3. Geometry parameter.

to the moving platform; r_c and O' are the radius and the center of the circumscribed circle of C_i respectively; r_a and O are the radius and the center of the circumscribed circle of A_i respectively; φ_{c1} is the angle of $\angle C_1 O' C_2$; and L_a is the length of $A_i B_i$. The other dimension parameters can be obtained by

$$\begin{cases} \varphi_{a1} = 2\text{asin}((r_c/r_a)\sin(\varphi_{c1}/2)) \\ \varphi_{a2} = (2\pi - 3\varphi_{a1})/3 \\ \varphi_{c2} = (2\pi - 3\varphi_{c1})/3 \\ L_c = L_a + (r_a\cos(\varphi_{a1}/2) - r_c\cos(\varphi_{c1}/2)) \end{cases},$$

https://doi.org/10.1017/S0263574714001969 Published online by Cambridge University Press

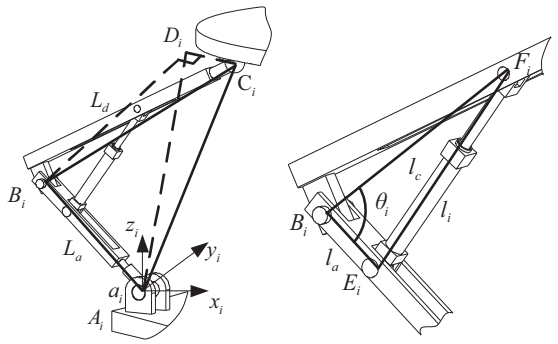

(a) (b)

Fig. 4. Branch and closed loop parameters.

where L_c is the length of B_iC_i; φ_{a1}, φ_{a2}, and φ_{c2} are the angles of $\angle A_5OC_6$, $\angle A_5OC_4$, and $\angle C_2O'C_3$ respectively.

The ith branch coordinate frame $\{a_i\}$ is established on joint center A_i, as shown in Fig. 4. The direction of the y_i-axis coincides with the revolute joint axis. The z_i-axis is vertical up.

Let $\boldsymbol{T}$ denotes the homogenous representation of the moving platform frame $\{o'\}$ relative to frame $\{o\}$, $\boldsymbol{T}_i$ is the transformation matrix of frame $\{a_i\}$ relative to frame $\{o\}$. The homogenous coordinates of point C_i in terms of frame $\{a_i\}$ can be given by

$$\bar{\boldsymbol{C}}_i^{a_i} = [\boldsymbol{T}_i]^{-1}\, T\bar{\boldsymbol{C}}_i^{o'}, \tag{1}$$

where $\bar{\boldsymbol{C}}_i^{o'}$ are the homogenous coordinates of point C_i in terms of frame $\{o'\}$.

Let D_i be the projection of point C_i in the x_iz_i-plane of frame $\{o\}$, the position vector of point D_i in terms of frame $\{a_i\}$ is given as

$$\boldsymbol{D}_i^{a_i} = \left[\left(\boldsymbol{C}_i^{a_i}\right)_{x_i} \quad 0 \quad \left(\boldsymbol{C}_i^{a_i}\right)_{z_i} \right]^T,$$

where $(\boldsymbol{C}_i^{a_i})_{x_i}$ and $(\boldsymbol{C}_i^{a_i})_{z_i}$ are the components along the x_i- and z_i-axes of vector $\boldsymbol{C}_i^{a_i}$ respectively.

The length of B_iD_i can be obtained from the result of Eq. (1),

$$L_d = \left(L_c^2 - \left(\boldsymbol{C}_i^{a_i}\right)_{y_i}^2\right)^{1/2}, \tag{2}$$

where, $(\boldsymbol{C}_i^{a_i})_{y_i}$ is the component along the y_i-axis of vector $\boldsymbol{C}_i^{a_i}$.

The following equations can be obtained based on the geometrical relationship

$$\begin{cases} \left(\boldsymbol{B}_i^{a_i}\right)_{x_i}^2 + \left(\boldsymbol{B}_i^{a_i}\right)_{z_i}^2 = L_a^2 \\ \left(\left(\boldsymbol{B}_i^{a_i}\right)_{x_i} - \left(\boldsymbol{D}_i^{a_i}\right)_{x_i}\right)^2 + \left(\left(\boldsymbol{B}_i^{a_i}\right)_{z_i} - \left(\boldsymbol{D}_i^{a_i}\right)_{z_i}\right)^2 = L_d^2 \end{cases}. \tag{3}$$

The above equations, combined with Eqs. (1) and (2), have two groups of solution. Since point C_i is always in the positive direction of the z-axis of frame $\{o\}$, the projection of point D_i should be in the positive direction of the z-axis in terms of frame $\{a_i\}$. Therefore, the rational solution of Eq. (3) is the one which has a smaller $(\boldsymbol{B}_i^{a_i})_{x_i}$, and the homogeneous coordinates of point B_i can be represented as

$$\bar{\boldsymbol{B}}_i = \boldsymbol{T}_i \bar{\boldsymbol{B}}_i^{a_i}.$$

The input angles θ_i $(i = 1,\ 2, ...6)$ can be obtained from the above results. The rotation angles of drive joints are determined by the input of prismatic joints in closed chain linkages, as shown

https://doi.org/10.1017/S0263574714001969 Published online by Cambridge University Press

in Fig. 4, and the length of l_i can be calculated from the geometrical relationship of closed chain linkages,

$$l_i = \left(l_a^2 + l_c^2 - 2l_a l_c \cos\theta_i\right)^{1/2}, \tag{4}$$

where l_a is the length of $B_i E_i$; l_c is the length of $B_i F_i$ in Fig. 4(b).

2.3. Velocity and acceleration analysis

The mapping from the velocity of each joint $\dot{\boldsymbol{\phi}}_i$ to the moving platform generalized velocity $\boldsymbol{V}_{\mathrm{H}}$ of the ith branch is expressed as

$$\boldsymbol{V}_{\mathrm{H}} = \boldsymbol{G}_i^{\mathrm{H}} \dot{\boldsymbol{\phi}}_i, \tag{5}$$

where

$$\boldsymbol{G}_i^{\mathrm{H}} = \begin{bmatrix} \boldsymbol{J}_1 & \boldsymbol{J}_2 & \cdots & \boldsymbol{J}_6 \end{bmatrix}; \boldsymbol{J}_i = \begin{pmatrix} \boldsymbol{S}_i \\ \boldsymbol{S}_i \times (\boldsymbol{P} - \boldsymbol{p}_i) \end{pmatrix},$$

where $\boldsymbol{S}_i$ is the direction of a revolute joint; $\boldsymbol{P}$ is the vector of origin $\{o'\}$; and $\boldsymbol{p}_i$ is the location of revolute joints.

The mapping from the moving platform generalized velocity $\boldsymbol{V}_{\mathrm{H}}$ to the generalized velocity of revolute joints $\dot{\boldsymbol{\theta}}$ is expressed as

$$\dot{\boldsymbol{\theta}} = \boldsymbol{G}_{\mathrm{H}}^{\theta} \boldsymbol{V}_{\mathrm{H}}, \tag{6}$$

where

$$\boldsymbol{G}_{\mathrm{H}}^{\theta} = \begin{pmatrix} \left[\boldsymbol{G}_1^{\mathrm{H}}\right]_{3:}^{-1} \\ \left[\boldsymbol{G}_2^{\mathrm{H}}\right]_{3:}^{-1} \\ \\ \left[\boldsymbol{G}_6^{\mathrm{H}}\right]_{3:}^{-1} \end{pmatrix}.$$

Hence, the mapping from $\dot{\boldsymbol{\theta}}$ to $\boldsymbol{V}_{\mathrm{H}}$ is expressed as

$$\boldsymbol{V}_{\mathrm{H}} = \boldsymbol{G}_{\theta}^{\mathrm{H}} \dot{\boldsymbol{\theta}}, \tag{7}$$

where $\boldsymbol{G}_{\theta}^{\mathrm{H}} = [\boldsymbol{G}_{\mathrm{H}}^{\theta}]^{-1}$.

By differentiating Eq. (7), the acceleration of the moving platform can be expressed as

$$\boldsymbol{A}_{\mathrm{H}} = \boldsymbol{G}_{\theta}^{\mathrm{H}} \ddot{\boldsymbol{\theta}} + \dot{\boldsymbol{\theta}}^{\mathrm{T}} H_{\theta}^{\mathrm{H}} \dot{\boldsymbol{\theta}}, \tag{8}$$

where $\boldsymbol{H}_{\theta}^{\mathrm{H}}$ is the second-order influence coefficient matrix of the system; $\ddot{\boldsymbol{\theta}}$ is the generalized angular acceleration of revolute joints; and $\boldsymbol{A}_{\mathrm{H}}$ is the generalized acceleration of the moving platform.

The above equations establish the relationships of velocity and acceleration between the moving platform and the driving revolute joints. As the rotation of the middle joint is driven by the translational drive, it is necessary to establish the velocity and acceleration mapping between the moving platform and prismatic joints in closed chain. By differentiating Eq. (4), the relationship between the revolute joints' velocities $\dot{\theta}_i$ and the prismatic joints' velocities $\dot{l}_i$ can be obtained:

$$\dot{\theta}_i = \frac{l_i}{l_a l_c \sin\theta_i} \dot{l}_i \quad (i = 1,\ 2 \cdots 6;). \tag{9}$$

The above equation can be written as

$$\dot{\boldsymbol{\theta}} = \boldsymbol{G}_l^{\theta} \dot{\boldsymbol{l}}, \tag{10}$$

https://doi.org/10.1017/S0263574714001969 Published online by Cambridge University Press

where

$$\boldsymbol{G}_l^{\theta} = \operatorname{diag}\left(\frac{l_1}{l_a l_c \sin\theta_1} \quad \frac{l_2}{l_a l_c \sin\theta_2} \quad \cdots \quad \frac{l_6}{l_a l_c \sin\theta_6} \right)_{6\times 6}.$$

According to Eqs. (7) and (10), the generalized velocity mapping of closed chain to the moving platform can be obtained as,

$$\boldsymbol{V}_{\mathrm{H}} = \boldsymbol{G}_l^{\mathrm{H}} \dot{\boldsymbol{l}}, \tag{11}$$

where $\boldsymbol{G}_l^{\mathrm{H}} = \boldsymbol{G}_{\theta}^{\mathrm{H}} \boldsymbol{G}_l^{\theta}$ is the first-order influence coefficient matrix of a foldable parallel mechanism driven by closed chain.

Similarly, the acceleration mapping from prismatic joints in closed chain linkages to the moving platform can be built by differentiating Eq. (11),

$$\boldsymbol{A}_{\mathrm{H}} = \boldsymbol{G}_{\theta}^{\mathrm{H}} \boldsymbol{G}_l^{\theta} \ddot{\boldsymbol{l}} + \dot{\boldsymbol{G}}_{\theta}^{\mathrm{H}} \boldsymbol{G}_l^{\theta} \dot{\boldsymbol{l}} + \boldsymbol{G}_{\theta}^{\mathrm{H}} \dot{\boldsymbol{G}}_l^{\theta} \dot{\boldsymbol{l}}. \tag{12}$$

By differentiating Eqs. (9) and (10), the accelerations of revolute and prismatic joints have the following relation:

$$\ddot{\boldsymbol{\theta}} = \boldsymbol{G}_l^{\theta} \ddot{\boldsymbol{l}} + \dot{\boldsymbol{l}}^{\mathrm{T}} \boldsymbol{H}_l^{\theta} \dot{\boldsymbol{l}}, \tag{13}$$

and the mapping of each branch:

$$\ddot{\theta}_i = \frac{l_i}{l_a l_c \sin\theta_i} \ddot{l}_i + h_i \dot{l}_i^2, \tag{14}$$

where

$$h_i = \frac{l_a l_c \sin\theta_i - l_i^2 \dfrac{\cos\theta_i}{\sin\theta_i}}{(l_a l_c \sin\theta_i)^2}.$$

Comparing with Eqs. (13) and (14), the second-order influence coefficient matrices of closed chain are obtained,

$$\boldsymbol{H}_l^{\theta} = \operatorname{diag}\begin{pmatrix} h_1 & h_2 & \cdots & h_6 \end{pmatrix}_{6\times 6\times 6}.$$

Substituting Eqs. (8), (10), and (13) into Eq. (12), the moving platform's acceleration is given as,

$$\boldsymbol{A}_{\mathrm{H}} = \boldsymbol{G}_{\theta}^{\mathrm{H}} \boldsymbol{G}_l^{\theta} \ddot{\boldsymbol{l}} + \dot{\boldsymbol{l}}^{T} \left[\boldsymbol{G}_l^{\theta}\right]^{T} \boldsymbol{H}_{\theta}^{\mathrm{H}} \boldsymbol{G}_l^{\theta} \dot{\boldsymbol{l}} + \dot{\boldsymbol{l}}^{T} \boldsymbol{G}_{\theta}^{\mathrm{H}} \otimes \boldsymbol{H}_l^{\theta} \dot{\boldsymbol{l}},$$

where the symbol $\otimes$ represents the Kronecker product between matrices. The acceleration mapping of closed chain to the moving platform can be obtained as

$$\boldsymbol{A}_{\mathrm{H}} = \boldsymbol{G}_l^{\mathrm{H}} \ddot{\boldsymbol{l}} + \dot{\boldsymbol{l}}^{\mathrm{T}} \boldsymbol{H}_l^{\mathrm{H}} \dot{\boldsymbol{l}}, \tag{15}$$

where $\boldsymbol{H}_l^{\mathrm{H}} = [\boldsymbol{G}_l^{\theta}]^{T} \boldsymbol{H}_{\theta}^{\mathrm{H}} \boldsymbol{G}_l^{\theta} + \boldsymbol{G}_{\theta}^{\mathrm{H}} \otimes \boldsymbol{H}_l^{\theta}$ is the second-order influence coefficient matrix of the foldable parallel mechanism driven by closed chain.

3. Directional Stiffness and its Extreme Value

3.1. Directional stiffness

Take 6-DOF mechanism for example, the only stiffness that we considered was the drive's stiffness $\boldsymbol{k} = \operatorname{diag}(k_1, k_2, \cdots k_6)$, where k_i is the stiffness of the ith branch drive. We also ignore the gravity and other forces acting on the link except the moving platform. Assume that the moving platform is suffering an external force $\boldsymbol{F}_{\mathrm{H}}$, and the mechanism is in a state of equilibrium. After the force changes

https://doi.org/10.1017/S0263574714001969 Published online by Cambridge University Press

$\delta \boldsymbol{F}_{\mathrm{H}} = \left(\begin{smallmatrix} \delta \boldsymbol{M} \\ \delta \boldsymbol{F} \end{smallmatrix}\right)$, the mechanism will get into a state of new equilibrium. The generalized displacement of the moving platform caused by the small force change is $\boldsymbol{\delta T} = \left(\begin{smallmatrix} \boldsymbol{\delta\theta} \\ \boldsymbol{\delta p} \end{smallmatrix}\right)$, where $\boldsymbol{\delta p} = [\,\delta p_x \quad \delta p_y \quad \delta p_z\,]^{\mathrm{T}}$ and $\delta\boldsymbol{\theta} = [\,\delta\theta_x \quad \delta\theta_y \quad \delta\theta_z\,]^{\mathrm{T}}$.

By the principle of virtual work, we can get $\boldsymbol{V}_{\mathrm{H}}^{\mathrm{T}}\boldsymbol{F}_{\mathrm{H}} + \dot{\boldsymbol{l}}^{\mathrm{T}}\boldsymbol{\tau} = 0$, and then

$$\dot{\boldsymbol{l}}^{\mathrm{T}}\boldsymbol{G}_l^{\mathrm{HT}}\boldsymbol{F}_{\mathrm{H}} + \dot{\boldsymbol{l}}^{\mathrm{T}}\boldsymbol{\tau} = 0, \tag{16}$$

where $\boldsymbol{V}_{\mathrm{H}}$ is the generalized velocity of the moving platform, $\dot{\boldsymbol{l}} = [\,l_1 \quad l_2 \quad \cdots\, l_6\,]^{\mathrm{T}}$ is the generalized velocity, and $\boldsymbol{\tau} = [\,\tau_1 \quad \tau_2 \quad \cdots\, \tau_6\,]^{\mathrm{T}}$ is the drive force of the ith branch.

Eliminate $\dot{\boldsymbol{l}}^{\mathrm{T}}$ from Eq. (16), and derive both sides, then it can be written as,

$$\delta\boldsymbol{G}_l^{\mathrm{HT}}\boldsymbol{F}_H + \boldsymbol{G}_l^{\mathrm{HT}}\delta\boldsymbol{F}_H + \delta\boldsymbol{\tau} = 0. \tag{17}$$

By the definition of the second-order influence matrix, we get:

$$\delta\boldsymbol{G}_l^{\mathrm{HT}}\boldsymbol{F}_{\mathrm{H}} = \sum_{i=1}^{6}\frac{\partial\boldsymbol{G}_l^{\mathrm{HT}}}{\partial l_i}\delta l_i\boldsymbol{F}_{\mathrm{H}} = \left(\boldsymbol{H}_l^{\mathrm{HT}} \otimes \boldsymbol{F}_{\mathrm{H}}\right)\delta\boldsymbol{l},$$

substitute it into Eq. (17), then

$$\left(\boldsymbol{H}_l^{\mathrm{HT}} \otimes \boldsymbol{F}_{\mathrm{H}}\right)\delta\boldsymbol{l} + \boldsymbol{G}_l^{\mathrm{HT}}\delta\boldsymbol{F}_H + \delta\boldsymbol{\tau} = 0. \tag{18}$$

As the drive stiffness is known as $k = \mathrm{diag}(k_1, k_2, \cdots k_6)$, we can get $\delta\boldsymbol{\tau} = -\boldsymbol{k}\delta\boldsymbol{l}$ and $\delta\boldsymbol{l} = \boldsymbol{G}_l^{\mathrm{H}-1}\delta\boldsymbol{T}$. Substitute these into Eq. (18), then we have:

$$\delta\boldsymbol{F}_H = \left(\boldsymbol{G}_l^{\mathrm{HT}}\right)^{-1}\left[\boldsymbol{k} - \left(\boldsymbol{H}_l^{\mathrm{HT}} \otimes \boldsymbol{F}_{\mathrm{H}}\right)\right]\left(\boldsymbol{G}_l^{\mathrm{H}}\right)^{-1}\delta\boldsymbol{T}. \tag{19}$$

So the stiffness matrix can be defined as

$$\boldsymbol{K} = \left(\boldsymbol{G}_l^{\mathrm{HT}}\right)^{-1}\left[\boldsymbol{k} - \left(\boldsymbol{H}_q^{\mathrm{HT}} \otimes \boldsymbol{F}_{\mathrm{H}}\right)\right]\left(\boldsymbol{G}_l^{\mathrm{H}}\right)^{-1}. \tag{20}$$

Set $\boldsymbol{F}_{\mathrm{H}} = 0$, then the stiffness matrix is expressed as

$$\boldsymbol{K} = \left(\boldsymbol{G}_l^{\mathrm{HT}}\right)^{-1}\boldsymbol{k}\left(\boldsymbol{G}_l^{\mathrm{H}}\right)^{-1} = \boldsymbol{G}_H^{l\mathrm{T}}\boldsymbol{k}\boldsymbol{G}_H^{l}. \tag{21}$$

The compliance matrix is the inverse of the stiffness matrix:

$$\boldsymbol{C} = \boldsymbol{G}_l^{\mathrm{H}}\boldsymbol{k}^{-1}\boldsymbol{G}_l^{\mathrm{HT}}. \tag{22}$$

Based on the above equation, the moving platform's translational and rotational stiffness along any direction can be deduced.

Assume the moving platform is suffering an external pure force without moment: $\delta\boldsymbol{F}_{\mathrm{H}} = \left(\begin{smallmatrix} \boldsymbol{0} \\ \delta\boldsymbol{F} \end{smallmatrix}\right)$. From Eq. (19), we can have

$$\begin{bmatrix} \boldsymbol{0} \\ \delta\boldsymbol{F} \end{bmatrix} = \begin{bmatrix} \boldsymbol{K}_1 & \boldsymbol{K}_2 \\ \boldsymbol{K}_3 & \boldsymbol{K}_4 \end{bmatrix}\begin{bmatrix} \delta\boldsymbol{\theta} \\ \delta\boldsymbol{p} \end{bmatrix}, \tag{23}$$

where the stiffness matrix $\boldsymbol{K}$ is separated as four 3×3 matrix $\left[\begin{smallmatrix} \boldsymbol{K}_1 & \boldsymbol{K}_2 \\ \boldsymbol{K}_3 & \boldsymbol{K}_4 \end{smallmatrix}\right]$.

It should be noted here that in Eq. (23), $\delta\boldsymbol{\theta}$ is not necessarily equal to zero, and $\delta\boldsymbol{p}$ is not necessarily be along $\delta\boldsymbol{F}$ either, for the translation of the moving platform caused by pure force may also couple with some translation.

https://doi.org/10.1017/S0263574714001969 Published online by Cambridge University Press

Deduce Eq. (23) further:

$$\begin{cases} \boldsymbol{K}_1\delta\boldsymbol{\theta} + \boldsymbol{K}_2\delta\boldsymbol{p} = \boldsymbol{0} \\ \boldsymbol{K}_3\delta\boldsymbol{\theta} + \boldsymbol{K}_4\delta\boldsymbol{p} = \delta\boldsymbol{F} \end{cases}.$$

Eliminating $\delta\boldsymbol{\theta}$ above, we have

$$\delta\boldsymbol{F} = \left(\boldsymbol{K}_4 - \boldsymbol{K}_3\boldsymbol{K}_1^{-1}\boldsymbol{K}_2\right)\delta\boldsymbol{p} = \boldsymbol{K}_p\delta\boldsymbol{p}. \tag{24}$$

As the directions of $\delta\boldsymbol{F}$ and $\delta\boldsymbol{p}$ are not coaxial, the projection of $\delta\boldsymbol{p}$ on $\delta\boldsymbol{F}$ is the displacement change along $\delta\boldsymbol{F}$. The translational direction stiffness along $\delta\boldsymbol{F}$, by symbol K_F, can get

$$K_F = \frac{|\delta\boldsymbol{F}|^2}{\delta\boldsymbol{p}^{\mathrm{T}}\delta\boldsymbol{F}} = \frac{|\delta\boldsymbol{F}|^2}{\delta\boldsymbol{F}^{\mathrm{T}}\left(\boldsymbol{K}_p^{-1}\right)^{\mathrm{T}}\delta\boldsymbol{F}}. \tag{25}$$

Setting $\delta\boldsymbol{F} = F\boldsymbol{f}$, $\boldsymbol{f}$ being the unit vector, Eq. (25) can be simplified as:

$$K_F = \boldsymbol{f}^{\mathrm{T}}\boldsymbol{K}_p^{\mathrm{T}}\boldsymbol{f}. \tag{26}$$

In a similar way, assume the moving platform is suffering an external pure moment without force $\delta\boldsymbol{F}_{\mathrm{H}} = \binom{\delta\boldsymbol{M}}{\boldsymbol{0}}$, then we can get similar equation as Eq. (24):

$$\delta\boldsymbol{M} = \left(\boldsymbol{K}_1 - \boldsymbol{K}_2\boldsymbol{K}_4^{-1}\boldsymbol{K}_3\right)\delta\boldsymbol{\theta} = \boldsymbol{K}_\theta\delta\boldsymbol{\theta}.$$

Then the rotational stiffness around $\delta\boldsymbol{M}$ can get:

$$K_M = \frac{|\delta\boldsymbol{M}|^2}{\delta\boldsymbol{M}^{\mathrm{T}}\left(\boldsymbol{K}_\theta^{-1}\right)^{\mathrm{T}}\delta\boldsymbol{M}}. \tag{27}$$

Setting $\delta\boldsymbol{M} = M\boldsymbol{m}$, $\boldsymbol{m}$ is the unit vector. The rotational stiffness around $\boldsymbol{m}$ can get

$$K_M = \boldsymbol{m}^{\mathrm{T}}\boldsymbol{K}_\theta^{\mathrm{T}}\boldsymbol{m}. \tag{28}$$

3.2. Extreme value of directional stiffness

Take translational stiffness, for example. In order to get the extreme stiffness when the direction $\boldsymbol{f}$ changes, the Lagrange multiplier method is used:

$$L = \boldsymbol{f}^{\mathrm{T}}\boldsymbol{K}_p^{\mathrm{T}}\boldsymbol{f} - \lambda\left(\boldsymbol{f}^{\mathrm{T}}\boldsymbol{f} - 1\right).$$

It should satisfy $\frac{\partial L}{\partial \boldsymbol{f}} = 0$; $\frac{\partial L}{\partial \lambda} = 0$, when L reaches the extreme value,

$$\begin{cases} 2\boldsymbol{f}^{\mathrm{T}}\boldsymbol{K}_p^{\mathrm{T}} - 2\lambda\boldsymbol{f}^{\mathrm{T}} = 0 \\ \boldsymbol{f}^{\mathrm{T}}\boldsymbol{f} - 1 = 0 \end{cases}.$$

Then we have $\boldsymbol{K}_p\boldsymbol{f} = \lambda\boldsymbol{f}$ and $K_F = \boldsymbol{f}^{\mathrm{T}}\boldsymbol{K}_p^{\mathrm{T}}\boldsymbol{f} = \lambda$, which means that all the eigenvalues of $\boldsymbol{K}_p$ are the extreme values of translational stiffness, and the corresponding eigenvector is the direction.

In the same way, the extreme value of rotational stiffness is all the eigenvalues of $\boldsymbol{K}_\theta$, and the corresponding eigenvector is the direction.

https://doi.org/10.1017/S0263574714001969 Published online by Cambridge University Press

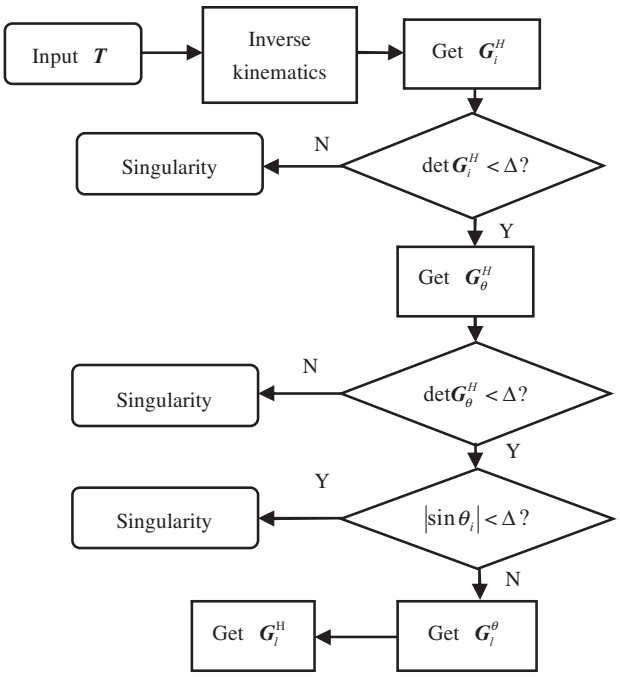

Fig. 5. Flowchart of singularity judgment.

3.3. Singularity judgment analyzed by stiffness

Singularity is closely related to the Jacobian matrix. As illustrated in Eqs. (5) and (6), the inverse of $\boldsymbol{G}_i^{\mathrm{H}}$ is necessary for building $\boldsymbol{G}_\theta^{\mathrm{H}}$. Therefore, if the rank of $\boldsymbol{G}_i^{\mathrm{H}}$ is deficient, the branch is in singularity. Therefore, the parallel mechanism is apparently in singularity. If $\boldsymbol{G}_i^{\mathrm{H}}$ is not deficient, $\boldsymbol{G}_\theta^{\mathrm{H}}$ can be built. However, if its rank is deficient, the mechanism is also in singularity. If $\boldsymbol{G}_l^\theta$ cannot be calculated by Eq. (10), then the branch is also in singularity, which causes the singularity of parallel mechanism. The judgments of singularity can be illustrated in Fig. 5. It should be noted that this method depends on the computer to calculate and judge nearly all the configurations in the workspace, and all the singularity configurations are not absolutely precise but are very close to the singularities. Δ is a positive real number that is close to zero.

The determinant of the first-order influence coefficient matrix is equal to zero when the mechanism is in a singular configuration. In practical applications, when the mechanism is near singularity, the kinematic performance may have already got poor. The singularities are classed into kinematic singularity and constrained singularity based on causation. When the kinematic singularity occurs, kinematic screws get linear correlation and the moving platform cannot move along or around any direction. Set the direction $\boldsymbol{A}(\boldsymbol{A} \neq \boldsymbol{0})$, from $\boldsymbol{G}_l^{\mathrm{H}}\dot{\boldsymbol{l}} = \boldsymbol{V}_{\mathrm{H}}$ we get $\boldsymbol{G}_l^{\mathrm{H}}\boldsymbol{A} = 0$ and $rank\boldsymbol{G}_l^{\mathrm{H}} < 6$. From Eq. (22), it satisfies $rank\boldsymbol{C} < 6$, which means that the compliance along $\boldsymbol{A}$, $\boldsymbol{C}A$ is zero, and the stiffness along $\boldsymbol{A}$ is infinite. When the constrained singularity occurs, constraint screws get linear correlation and the moving platform can achieve additional DOF along some directions when all the six drives are locked. Set the direction $\boldsymbol{B}(\boldsymbol{B} \neq \boldsymbol{0})$, considering $\dot{\boldsymbol{l}} = \boldsymbol{G}_{\mathrm{H}}^l\boldsymbol{V}_{\mathrm{H}}$, we get $\boldsymbol{G}_{\mathrm{H}}^l\boldsymbol{B} = \boldsymbol{0}$ and $rank\boldsymbol{G}_{\mathrm{H}}^l < 6$. Considering Eq. (21), $rank\boldsymbol{K} < 6$ can be obtained. It means that the stiffness along $\boldsymbol{B}$, $\boldsymbol{K}B$ is zero. Both kinds of singularities may occur at the same position and orientation, and the difference is in their directions.

4. Examples

The dimensions of the mechanism are set as $r_c = 1.75$ m; $r_a = 2.5$ m; $\varphi_{c1} = 110^\circ$; $L_a = 1.5$ m; $l_a = 1.479$ m; and $l_c = 1.479$ m.

Spheroidal coordinate is used to illustrate the stiffness of moving platform in all directions. It represents the direction and the norm of translational and rotational stiffness, shown in Figs. 6 and 7. The distance from the points on the surface to the origin is the value of stiffness, and the vectors

https://doi.org/10.1017/S0263574714001969 Published online by Cambridge University Press

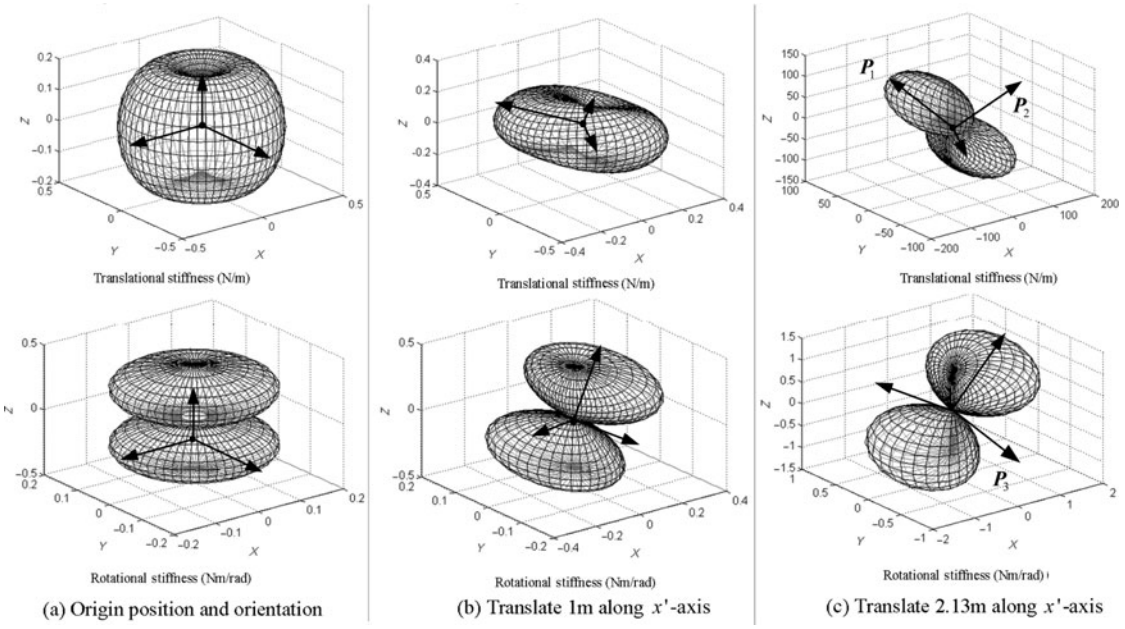

Fig. 6. The directional stiffness as the moving platform translates.

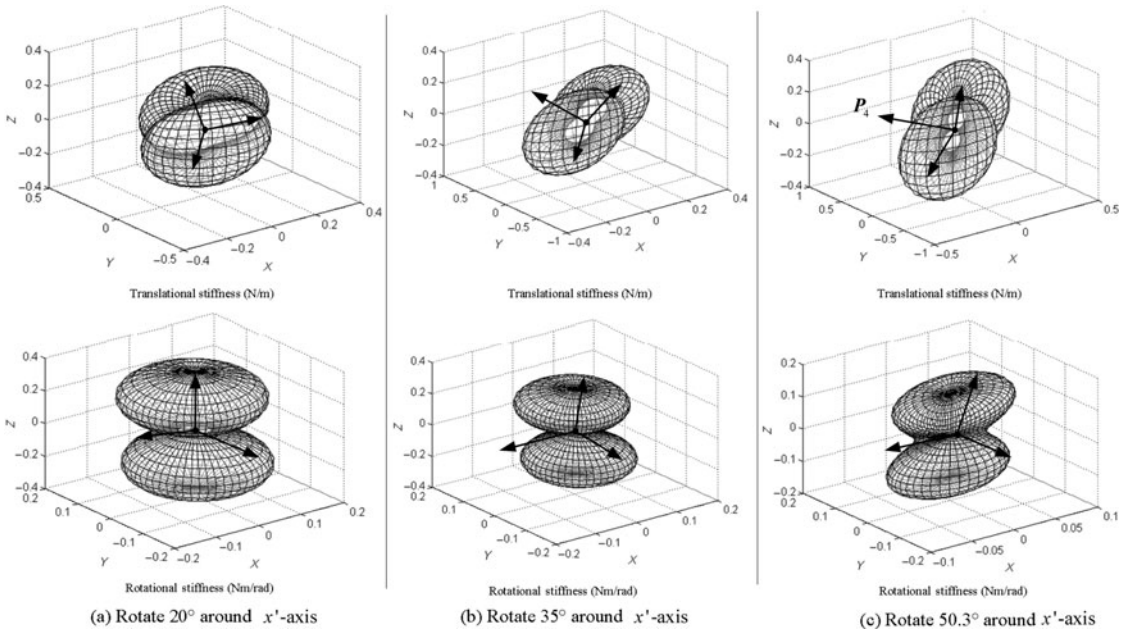

Fig. 7. The directional stiffness as the moving platform rotates.

of the points are the directions. The arrows in these figures illustrate extreme stiffness. As the main destination is singularity analysis, it might as well set the drive stiffness as 1 N/m.

At the initial position and orientation (moving platform is in the middle place, and horizontal, the height is 2.5 m), the translational stiffness along all directions is illustrated in Fig. 6 (a). It can be seen that the distribution of translational stiffness is uniform. However, the distribution of rotational stiffness is not uniform, especially when the stiffness around x', y' directions are smaller. The directional stiffness is illustrated in Fig. 6(b) and (c) when the moving platform moves 1 m and 2.13 m (where it is very close to singularity) along the x'-axis. As the mechanism gets close to the boundary of the workspace, it gets close to singularity as well, and the directional stiffness along some directions (such as $\boldsymbol{P}_1$) get close to infinite (200 times than the drive stiffness 1 N/m). Along

https://doi.org/10.1017/S0263574714001969 Published online by Cambridge University Press

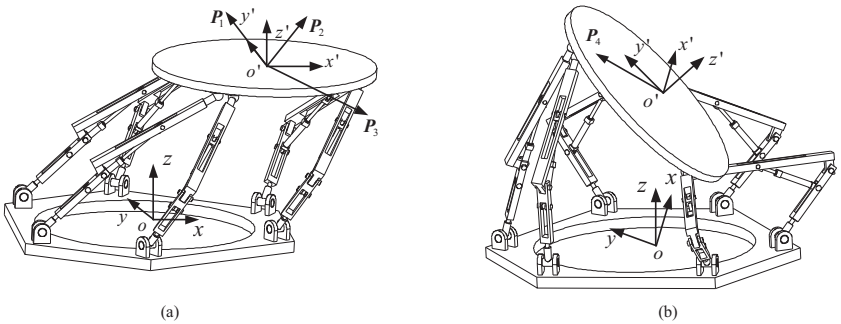

Fig. 8. The singularity configurations and the directions.

these directions the mechanism cannot move, which means kinematic singularity. On the other hand, along some directions, such as translational stiffness along $\boldsymbol{P}_2$ and rotational stiffness around $\boldsymbol{P}_3$, the value gets close to zero, and the mechanism loses its constraints, which means constrained singularity. Therefore, the configuration is in both kinematic and constrained singularity, and the difference is the directions along (or around) which singularity occurs. The singularity configuration is shown in Fig. 8 (a).

Figures 7(a), (b), and (c) illustrate the directional stiffness along and around the directions when the moving platform rotates 20°, 35°, and 50.3° around x' of $\{o'\}$ coordinate respectively. It gets very close to singularity when it rotates 50.3°. The moving platform lost its constraints along some directions, such as $\boldsymbol{P}_4$, for the stiffness along these directions is close to zero. The mechanism is in constrained singularity only. The rotational stiffness changes are steady, and no singularity occurs around all these directions. The singularity configuration is shown in Fig. 8(b)

5. Conclusions

The mechanism which is used as a heavy load ship-based stabilized platform has been analyzed. Based on inverse kinematics, the first- and second-order influence matrices of the closed loop drive mechanism have been deduced. The stiffness matrix considering changes in the configuration of mechanism has been built based on virtual work principle. After that translational and rotational stiffness along any directions are deduced. Moreover, the extreme values of translational and rotational stiffness are obtained according to the separation of stiffness matrix. At last, the spheroidal coordinates were used to illustrate directional stiffness. In this way, the singularity was analyzed using the data of directional stiffness.

It is important that the way to analyze the singularity is visual and accessible. The directions can be obtained to illustrate the directions the moving platform cannot move or lost its constraints. It will make clear as to how the kinematic situation will be when the mechanism gets close to singularity.

Acknowledgment

This work was supported by the National Natural Science Foundation of China (Grant Nos. 51375420 and 51105322).

References

1. J. A. Keller and E. C. Smith, "Experiment and theoretical correlation of helicopter rotor blade-droop stop impacts," *J. Aircr.* **36**(2), 443–450 (1999).
2. J. Ma, P. Yang and G. Li, "Simulation study of ship's movement regularity and anti-rolling technology under high-wave-level environment," *Ship Eng.* **28**(2), 24–29 (2006).
3. M. M. Kamel, "Bifurcation analysis of a nonlinear coupled pitch-roll ship," *Math. Comput. Simul.* **73**(5), 300–308 (2007).
4. Z. Huang, Y. S. Zhao and T. S. Zhao, *Advanced Spatial Mechanism* (Higher Education Press, Beijing, China, 2006) pp. 169–212, 239–276.
5. Z. Huang, L. F. Kong and Y. F. Fang, *"Mechanism Theory and Control of Parallel Robot"* (China Machine Press, Beijing, China, 1997).

https://doi.org/10.1017/S0263574714001969 Published online by Cambridge University Press

6. B. Dasgupta and T. S. Mruthyunjaya, "Closed-form dynamic equations of the general Stewart platform through the Newton–Euler approach," *Mech. Mach. Theory* **33**(7), 993–1012 (1998).
7. T. Langbecker and F. Albermani, "Kinematic and non-linear analysis of foldable barrel vaults," *Eng. Struct.* **23**, 158–171 (2001).
8. C. M. Gosselin and J. Angeles, "Singularity analysis of closed-loop kinematic chains," *IEEE Trans. Robot. Autom.* **6**(3), 281–290 (1990).
9. J. S. Zhao, J. Y. Wang, F. L. Chu and J. S. Dai, "Structure synthesis and statics analysis of a foldable stair," *Mech. Mach. Theory* **46**(7), 998–1015 (2011).
10. D. Zlatanov, R. G. Fenton and B. Benhabib, "A unifying framework for classification and interpretation of mechanism singularities," *Trans. ASME J. Mech. Des.* **117**, 566–572 (1995).
11. D. Zlatanov, R. G. Fenton and B. Benhabib, "Identification and classification of the singular configurations of mechanisms," *Mech. Mach. Theory* **33**(6), 743–760 (1998).
12. J. Chung, T. S. Jong, J. Y. Byung, K. K. Whee and H. L. Sang, "Implementation of a Foldable 3-DOF Master Device to Handle a Large Glass Plate," *Proceedings of the IEEE/RSJ International Conference on Intelligent Robots and Systems*, St. Louis, MO (2009) pp. 741–747.
13. J. Chung, J. Y. Byung and O. Sung, "A foldable 3-DOF parallel mechanism with application to a flat-panel TV mounting device," *IEEE Trans. Robot.* **25**(5), 1214–1221 (2009).
14. S. Joshi and L. W. Tsai, "A comparison study of two 3-DOF parallel manipulators: One with three and the other with four supporting legs," *IEEE Trans. Robot. Autom.* **19**(2), 200–209 (2003).
15. H. Shin, S. Kim, J. Jeong and J. Kim, "Stiffness enhancement of a redundantly actuated parallel machine tool by dual support rims," *Int. J. Precis. Eng. Manuf.* **13**(9), 1539–1547 (2012).
16. J. S. Dai and T. S. Zhao, "Stiffness characteristics and kinematics analysis of two-link elastic underactuated manipulators," *J. Robot. Syst.* **19**(4), 169–176 (2002).